Numerical Studies of Electromagnetic Instabilities in Intense Charged Particle Beams with Large Energy Anisotropy*

Edward A. Startsev, Ronald C. Davidson and Wei-li Lee
Plasma Physics Laboratory, Princeton University, Princeton, New Jersey, 08543 USA

Abstract

In intense charged particle beams with large energy anisotropy, free energy is available to drive transverse electromagnetic Weibel-type instabilities. Such slow-wave transverse electromagnetic instabilities can be described by the so-called Darwin model, which neglects the fast-wave portion of the displacement current. The Weibel instability may also lead to an increase in the longitudinal velocity spread, which would make the focusing of the beam difficult and impose a limit on the minimum spot size achievable in heavy ion fusion experiments. This paper reports the results of recent numerical studies of the Weibel instability using the Beam Eigenmode And Spectra (bEASt) code for space-charge-dominated, low-emittance beams with large tune depression. To study the nonlinear stage of the instability, the Darwin model is being developed and incorporated into the Beam Equilibrium Stability and Transport(BEST) code.

INSTABILITY MECHANISM

To illustrate the physical mechanism for the electromagnetic Weibel-type instability [1–5] we consider a charged particle beam confined inside a circular conducting pipe of radius r_w by an external linear force $\mathbf{F} = -m_b\omega_f^2\mathbf{x}_\perp$ in the smooth-focusing approximation. For simplicity, the analysis is carried out in the beam frame ($V_b = 0$). The beam is confined in the transverse direction provided $\hat{\omega}_{pb}^2/2\omega_f^2 < 1$. Here, $\hat{\omega}_{pb}^2 = 4\pi e_b^2\hat{n}_b/m_b$ is the on-axis ($r = 0$) plasma frequency-squared, and ω_f is the average oscillation frequency of a beam particle with mass m_b and charge e_b in the applied focusing field. It follows from the numerical analysis that the fastest growing modes correspond to rigid rotations of the beams slices with $\delta J_\theta \sim r$ for $\hat{\omega}_{pb}^2/2\omega_f^2 \to 1$. The growth rate is an increasing function of $k_z r_b$ and approaches a maximum value for $k_z^2 r_b^2 \gg 1$. Therefore, in leading order, the perturbed magnetic field is given approximately by $\delta\mathbf{B} \simeq ik_z\delta A_\theta \mathbf{e}_r$ for $k_z^2 r_b^2 \gg 1$. From Maxwell's equations it follows that

$$\delta A_\theta(\mathbf{x},t) = \hat{A}_\theta \frac{r}{r_b} e^{i(k_z z-\omega t)}. \tag{1}$$

The longitudinal equation of motion for a beam particle becomes

$$\ddot{z} = -\frac{e_b}{m_b}\frac{v_\theta}{c}\delta B_r = -ik_z\frac{e_b}{m_b}\hat{A}_\theta\frac{r(t)v_\theta(t)}{cr_b}e^{i(k_z z_0-\omega t)}. \tag{2}$$

In the smooth-focusing approximation, the unperturbed motion is in a cylindrically-symmetric potential $U(r)$, and therefore the angular momentum is conserved $r(t)v_\theta(t) = const.$ Integrating Eq. (2) with respect to time t, we obtain

$$z(t) = i\frac{k_z}{\omega^2}\frac{e_b}{m_b}\hat{A}_\theta\frac{r(t)v_\theta(t)}{cr_b}e^{i(k_z z_0-\omega t)} = \frac{v_\theta}{\omega^2}\frac{e_b\delta B_r}{m_b c}. \tag{3}$$

The average axial displacement is given by $\langle z\rangle \sim \langle v_\theta\rangle = 0$, and therefore the density perturbation $\delta n_b = -\bar{n}_b\partial\langle z\rangle/\partial z = 0$ is zero. For the current perturbations we obtain,

$$\frac{\partial\delta J_\theta}{\partial t} + \frac{\partial}{\partial z}\left(e_b\bar{n}_b\frac{\partial\langle v_\theta z\rangle}{\partial t}\right) = 0,$$
$$\delta J_\theta = -e_b\bar{n}_b\frac{\partial\langle v_\theta z\rangle}{\partial z} = -\frac{e_b^2\bar{n}_b}{m_b c}\frac{\langle v_\theta^2\rangle}{\omega^2}\frac{\partial\delta B_r}{\partial z}. \tag{4}$$

Substituting Eq. (4) into Maxwell's equation $\partial\delta B_r/\partial z = 4\pi\delta J_\theta/c$, we obtain the dispersion relation

$$1 = -\frac{\bar{\omega}_{pb}^2}{\omega^2}\frac{\langle v_\theta^2\rangle}{c^2}, \tag{5}$$

where $\bar{\omega}_{pb}^2 = 4\pi e_b^2\bar{n}_b/m_b$ is the average beam plasma frequency-squared. Noting that $T_{\perp b} = m_b\langle v_\theta^2 + v_r^2\rangle/2 = m_b\langle v_\theta^2\rangle$ we can express the growth rate as

$$\gamma = \bar{\omega}_{pb}\sqrt{\frac{T_{\perp b}}{m_b c^2}} = \frac{\bar{\omega}_{pb}}{\sqrt{2}}\frac{v_{\perp b}^{th}}{c} \approx 0.71\frac{v_{\perp b}^{th}}{c}, \tag{6}$$

where $v_{\perp b}^{th} = \sqrt{2T_{\perp b}/m_b}$ is the transverse thermal velocity.

DESCRIPTION OF BEAM EIGENMODE AND SPECTRA (BEAST) CODE

For an arbitrary equilibrium distribution one cannot solve the stability problem analytically and must employ numerical techniques. To investigate the stability properties numerically, we make use of the linear eighenmode method, which searches for the roots of the matrix dispersion relation, as implemented in the Beam Eigenmode and Spectra (bEASt) code. We briefly outline here the derivation of the matrix dispersion relation for the Weibel-like instability [5] in intense particle beams for electromagnetic perturbations of the form

$$\delta A_\theta(\mathbf{x},t) = \widehat{\delta A}(r)e^{i(k_z z-\omega t)} \tag{7}$$

about the thermal equilibrium distribution with temperature anisotropy ($T_{\perp b} > T_{\|b}$) described *in the beam frame*

* Research supported by the U.S.Department of Energy.

($V_b = 0$ and $\gamma_b = 1$) by the self-consistent axisymmetric Vlasov equilibrium

$$f_b^0(r,\mathbf{p}) = \frac{\widehat{n}_b}{(2\pi m_b)^{3/2} T_{\perp b} T_{||b}^{1/2}} \exp\left(-\frac{H_\perp}{T_{\perp b}} - \frac{p_z^2}{2m_b T_{\|b}}\right). \tag{8}$$

Here, $H_\perp = p_\perp^2/2m_b + (1/2)m_b\omega_f^2(x^2+y^2) + e_b\phi^0(r)$ is the single-particle Hamiltonian for transverse particle motion, and $\omega_f = const.$ is the transverse focusing frequency. Perturbations are expanded in terms of the complete set of vacuum eigenfunctions $\widehat{\delta A}(r) = \sum_n \alpha_n A_n(r)$, where $A_n(r) = A_n J_1(\lambda_n r/r_w)$ and $J_1(\lambda_n) = 0$. Using the method of characteristics, analysis of the linearized Vlasov-Maxwell equations leads to an infinite dimension matrix dispersion equation [5]

$$\sum \alpha_n D_{n,m}(\omega) = 0, \tag{9}$$

where the elements of the dispersion matrix are defined by

$$D_{n,n'}(\omega) = \frac{J_2^2(\lambda_n)}{2}(\lambda_n^2 + k_z^2 r_w^2 - r_w^2\frac{\omega^2}{c^2})\delta_{n,n'} + \chi_{n,n'}(\omega). \tag{10}$$

Here, $\chi_{n,n'}$ is the beam-induced susceptibility. The beam-induced susceptibility for low-frequency modes $\omega \ll \omega_f$ is given by [5]

$$\chi_{n,n'}(\omega) = \frac{\hat{\omega}_{pb}^2}{c^2} \times \left\{1 - \frac{T_{||}}{T_\perp}\left[1 + \frac{\omega}{k_z v_{||}^{th}} Z\left(\frac{\omega}{k_z v_{||}^{th}}\right)\right]\right\} Q_{n,n'}, \tag{11}$$

where

$$Q_{n,n'} = \int \frac{dP_\theta P_\theta^2}{m_b^2\omega_r}\frac{dH_\perp}{T_{\perp b}^2}\exp\left[-\frac{H_\perp}{T_{\perp b}}\right](I_n)^* I_{n'}. \tag{12}$$

Here, P_θ is the canonical angular momentum, $\hat{\omega}_{pb}^2 = 4\pi e_b^2 \hat{n}_b/m_b$ is the on-axis plasma frequency-squared, and $v_{||b}^{th} = \sqrt{2T_{||b}/m_b}$. The orbit integral I_n is defined by

$$I_n(H_\perp, P_\theta) = \int_0^{T_r} \frac{d\tau}{T_r} J_1\left[\frac{\lambda_n r(\tau)}{r(\tau)}\right], \tag{13}$$

where $r(\tau)$ is the transverse orbit in the equilibrium field configuration.

The Beam Eigenmode and Spectra (bEASt) code solves Eq. (9) in several steps. First, the particle orbit $r(\tau)$ in the equilibrium field configuration is calculated for one complete oscillation period T_r, and the frequency $\omega_r(H_\perp, P_\theta)$ is obtained. Next, the orbit integrals in Eq. (13) are calculated and used in the integrations needed to obtain the matrix elements $Q_{n,n'}$ [Eq. (12)]. Finally, the matrix elements $Q_{n,n'}$ are used in Eqs. (11) and (10) during the search for the complex eigenfrequency ω producing the dispersion matrix $D_{n,n'}(\omega)$ with zero eigenvalue [Eq. (9)]. The typical number of particle trajectories used in the calculations is 300, with 16 time steps during one oscillation period T_r, which is significantly less than the number of particles and times steps used in PIC simulations. For moderately intense beams with $\bar{\nu}/\nu_0 > 0.4$, the rank of the dispersion matrix $N = 6$ is sufficient for convergence of the results. Here $\bar{\nu}/\nu_0 = v_\perp^{thb}/r_b\omega_f$ is the normalized depressed tune.

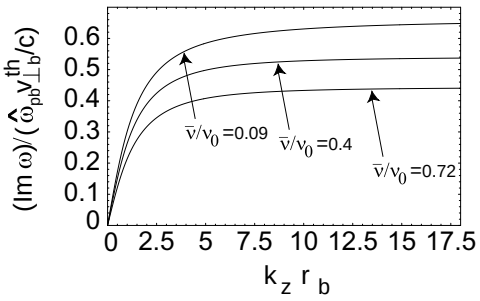

Figure 1: Plot of normalized growth rate $(Im\omega)/(\widehat{\omega}_{pb}v_{\perp b}^{th}/c)$ versus $k_z r_b$ for normalized skin depth $c/r_b\widehat{\omega}_{pb} = 100$ and several values of the normalized depressed tune $\bar{\nu}/\nu_0 = 0.09, 0.4, 0.72$ and $T_{||b}/T_{\perp b} = 0$.

NUMERICAL RESULTS

Typical numerical results obtained using the bEASt code for the case where $r_w = 3r_b$, are shown in Figures 1-5. In Figures 1-3, $T_{||b}/T_{\perp b} = 0$. Figure 1 shows the normalized growth rate $(Im\omega)/(\widehat{\omega}_{pb}v_{\perp b}^{th}/c)$ plotted versus $k_z r_b$ for normalized skin depth $c/r_b\widehat{\omega}_{pb} = 100$ and several values of the normalized depressed tune $\bar{\nu}/\nu_0 = 0.09, 0.4, 0.72$. The growth rate is an increasing function of $k_z r_b$ and approaches a maximum value for $k_z^2 r_b^2 \gg 1$, as indicated in the Introduction. The normalized maximum growth rate $(Im\omega)_{max}/(\omega_f^2 r_w/c)$, plotted versus the normalized depressed tune $\bar{\nu}/\nu_0$, is shown in Fig. 2. Note, that the maximum growth rate $(Im\omega)_{max} = 0.15\omega_f^2 r_w/c$ is achieved for moderately intense beams with $\bar{\nu}/\nu_0 \approx 0.73$. Figure 3 shows the normalized eigenfunctions $\delta\widehat{A}_\theta(r)$ for the most unstable mode versus r/r_w, corresponding to several values of the normalized depressed tune $\bar{\nu}/\nu_0 = 0.09, 0.4, 0.72$. Here, $k_z r_b = 20$ and $c/r_b\widehat{\omega}_{pb} = 100$. Also shown are plots of the normalized density profile $n_b(r)/n_b(0)$ for $\bar{\nu}/\nu_0 = 0.09, 0.4, 0.72$. Evidently, as the beam intensity increases ($\bar{\nu}/\nu_0 \to 0$) the eigenfunctions become localized near the beam edge and N increases sharply, indicating the need for a different expansion basis. Also note, that for $\bar{\nu}/\nu_0 \to 0$ the eigenfunction inside the beam becomes linear with $\delta\widehat{A}_\theta(r) \sim r$ [Eq. (1)], which corresponds to rigid rotations of the beams slices with $\delta J_\theta \sim r$. An important characteristic of the instability is the longitudinal threshold temperature $T_{||b}^{th}$ for the onset of instability normalized to the ratio of the transverse temperature to the normalized skin depth-squared $T_{\perp b}r_b^2\widehat{\omega}_{pb}^2/c^2$. This quantity is plotted in Fig. 4 versus the normalized skin depth $c/r_b\widehat{\omega}_{pb}$ for $\bar{\nu}/\nu_0 = 0.09, 0.4, 0.72$. Note from Fig. 4 that

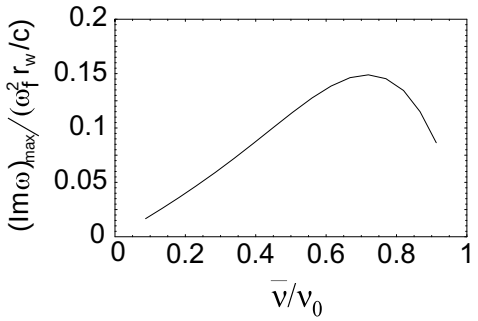

Figure 2: Plot of normalized maximum growth rate $(Im\omega)_{max}/(\omega_f^2 r_w/c)$ versus the average depressed tune $\bar{\nu}/\nu_0$ for $T_{||b}/T_{\perp b} = 0$.

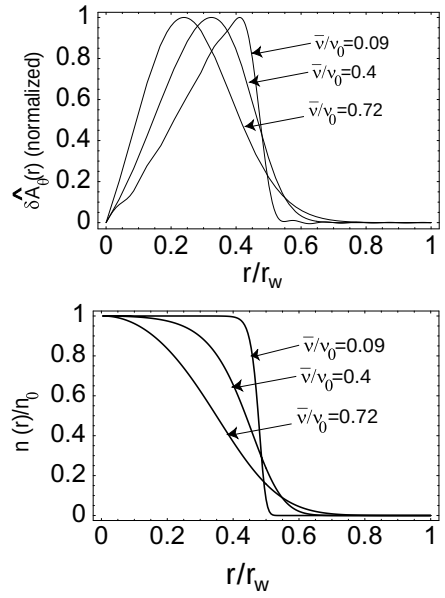

Figure 3: Plots of the normalized eigenfunctions $\delta\widehat{A}_\theta(r)$ for the most unstable mode versus r/r_w, corresponding $\bar{\nu}/\nu_0 = 0.09, 0.4, 0.72$. Here, $T_{||b}/T_{\perp b} = 0$, $k_z r_b = 20$ and $c/r_b\widehat{\omega}_{pb} = 100$. Also shown are plots of the normalized density profile $n_b(r)/n_b(0)$ for $\bar{\nu}/\nu_0 = 0.09, 0.4, 0.72$.

the normalized threshold temperature is a weak function of the normalized skin depth for $c/r_b\widehat{\omega}_{pb} \geq 3$, and is plotted in Fig. 5 as a function of the normalized tune depression $\bar{\nu}/\nu_0$ for the representative skin depth $c/r_b\widehat{\omega}_{pb} = 100$.

CONCLUSIONS

We have generalized the classical Weibel-type instability to the case of an intense charged particle beam with anisotropic temperature $(T_{||b}/T_{\perp b} < 1)$ including the important effects of finite transverse geometry and beam space-charge. The bEASt code, which solves the matrix dispersion relation for electromagnetic perturbations in intense particle beams, has been used to investigate the

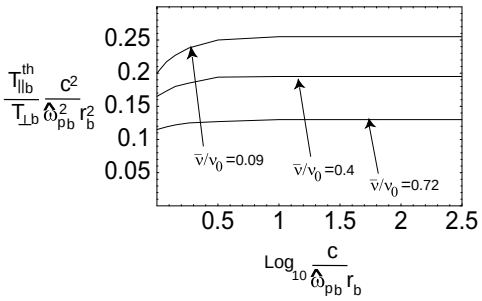

Figure 4: The normalized longitudinal threshold temperature $(T^{th}_{||b}/T_{\perp b})c^2/r_b^2\widehat{\omega}^2_{pb}$ for the onset of instability is plotted versus the normalized skin depth $c/r_b\widehat{\omega}_{pb}$ for $\bar{\nu}/\nu_0 = 0.09, 0.4, 0.72$.

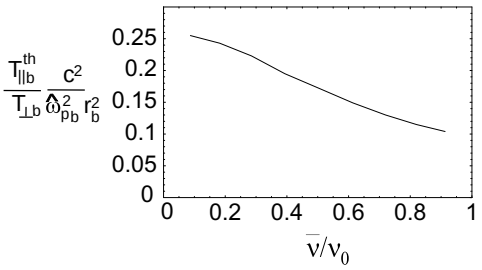

Figure 5: The normalized longitudinal threshold temperature $(T^{th}_{||b}/T_{\perp b})c^2/r_b^2\widehat{\omega}^2_{pb}$ for the onset of instability is plotted versus the normalized tune depression $\bar{\nu}/\nu_0$ for normalized skin depth $c/r_b\widehat{\omega}_{pb} = 100$.

stability properties of intense charged particle beams with large temperature anisotropy $(T_{||b}/T_{\perp b} \ll 1)$ over a wide range of normalized tune depression, $0.1 < \bar{\nu}/\nu_0 < 1$. It is found that even a small longitudinal temperature, $T^{th}_{||b}/T_{\perp b} \approx 0.25 r_b^2\widehat{\omega}^2_{pb}/c^2 \sim (v^{th}_{\perp b}/c)^2 \ll 1$, is large enough to stabilize the Weibel instability. The presence of this threshold is due to the finite transverse geometry of the charged particle beam. In future investigations, we plan to carry out detailed kinetic simulations of the Weibel instability employing a version of the BEST code modified to include transverse electromagnetic effects by incorporating a Darwin model that neglects the transverse displacement current [6]. This will permit detailed investigations of the both the linear and nonlinear phases of the instability.

REFERENCES

[1] E. S. Weibel, Phys. Rev. Lett. **2**, 83 (1959).

[2] R. C. Davidson, D. A. Hammer, I. Haber and C. E. Wagner, Phys. Fluids **15**, 317 (1972).

[3] R. Lee and M. Lampe, Phys. Rev. Lett. **31**, 1390 (1973).

[4] C. A. Kapetanakos, Appl. Phys. Lett. **25**, 484 (1974).

[5] E. A. Startsev and R. C. Davidson, Physics of Plasmas **10**, 4829 (2003).

[6] W. W. Lee, R. C. Davidson. E. A. Startsev and H. Qin, Nucl. Instr. and Meth. A, in press (2005).